JMEPEG (2009) 18:441–445
DOI: 10.1007/s11665-008-9312-7

1059-9495/$19.00

Fourier Thermal Analysis of the Eutectic Formed in Pb-Sn Alloys

H. Cruz, M. Ramírez-Argaez, A. Juarez, A. Garcia, and C. González-Rivera

(Submitted February 28, 2008; in revised form September 1, 2008)

The effect of the presence of two different primary phases on the microstructural characteristics and solidification kinetics of Pb-Sn eutectic was analyzed using Fourier thermal analysis method (FTA) and microstructural characterization. Three Pb-Sn alloys, a hypoeutectic, an eutectic, and a hypereutectic alloy, were melted in an electric furnace under an argon atmosphere and poured into sand molds. Cooling curves were obtained and numerically processed using FTA. Microstructural observations of the probes indicate a lamellar morphology for the eutectic microconstituent of the hypereutectic alloy; the eutectic alloy shows the presence of both lamellar and anomalous eutectic and the hypoeutectic alloy shows only the presence of anomalous eutectic. FTA results indicate that in the case of the probes showing the presence of anomalous eutectic, there is a primary eutectic formed during recalescence at high undercooling and a secondary eutectic yielded at low undercooling at the eutectic plateau temperature. This result shows that the cause behind the observed differences in the eutectic morphologies of the experimental alloys lies on the nucleating ability of the primary phase available as a potential substrate for nucleation of the eutectic microconstituent.

Keywords anomalous eutectic, Fourier thermal analysis, Pb-Sn eutectic, solidification kinetics

1. Introduction

Several alloy systems of commercial interest show the formation of two main microconstituents during solidification: a primary solid solution and an eutectic. Depending on the nature of the primary phase formed previously during solidification and on its ability to act as nucleating agent of the eutectic microconstituent, the eutectic can show changes in solidification kinetics and morphology, which in turn could affect the properties of the solidification product.

In binary alloy systems showing phase diagrams which includes two terminal solid solutions and one eutectic transformation such as Pb-Sn, Al-Zn, Bi-Cd, and others (Ref 1-3), it has been found that one of the two primary phases can act as a good nucleation substrate while the other acts as a substrate unable to promote nucleation of the eutectic, causing morphological changes on it. This effect has been named nonreciprocal nucleation (Ref 4). Pb-Sn alloy system exhibits a phase diagram with proper characteristics to explore the effect of the presence of two different primary phases on the solidification kinetics and microstructural characteristics of an eutectic microconstituent. In this binary system, the nonreciprocal nucleation has been related to morphological changes in the eutectic microconstituent (Ref 4, 5), which have been associated to a specific degree of undercooling. These changes have been confirmed in more recent works (Ref 6, 7), where it has been found that by increasing undercooling of eutectic Pb-Sn alloy before solidification, eutectic morphology changes from lamellar to anomalous. The mechanisms explaining formation of anomalous eutectic in undercooled melts are still under discussion (Ref 8).

Recently, computer aided cooling curve analysis (CA-CCA) methods have been used to study solidification kinetics of various alloy systems of metallurgical interest. Newton thermal analysis (NTA) and Fourier thermal analysis (FTA) are the most representative techniques. It has been found that FTA is the most reliable method because it takes into account the presence of thermal gradients in the probe using data acquired from two thermocouples located at two different radial positions within the sample to obtain the zero baseline curve. Fundamentals, limitations, and implementation of this method have been discussed elsewhere (Ref 9-12).

The purpose of this work was to study the effect of the presence of two different primary phases on the microstructural characteristics and solidification kinetics of Pb-Sn eutectic using cooling curve analysis, FTA method, and microstructural characterization.

2. Experimental Procedure

In order to explore the effect of the primary phase previously formed on the morphology and solidification kinetics showed by the eutectic microconstituent, an hypoeutectic alloy Pb-40wt.%Sn and an hypereutectic alloy Pb-80wt.%Sn were used in this work. In order to analyze the evolution of the

H. Cruz, M. Ramírez-Argaez, A. Garcia and **C. González-Rivera**, Departamento de Ingeniería Metalúrgica, Facultad de Química, UNAM, Av. Universidad 3000 Cd. Universitaria 04510, México D.F., México; and **A. Juarez**, Facultad de Ingeniería Mecánica y Eléctrica, Universidad Autónoma de Nuevo León, Pedro de Alba s/n, Ciudad Universitaria, San Nicolás de los Garza, Nuevo León C.P. 66450, México. Contact e-mails: carlosgrunam@yahoo.com and carlosgr@servidor.unam.mx.

eutectic constituent in the absence of any primary phase, an alloy with the eutectic composition 61.9 wt.% Sn was also included. Pre-weighed quantities of 99.8 wt.% Pb and 99.99 wt.% Sn were melted in an electric furnace under an Ar gas atmosphere. A total mass of 288.8, 263.7, and 242 g for the hypoeutectic, eutectic, and hypereutectic molten alloys, respectively, were poured with minimum turbulence directly into silicate/CO_2 bonded sand moulds. Dimensions of the top and bottom insulated moulds were 2 cm inner diameter, 10 cm height, and 2.5 cm of wall thickness. Moulds were surrounded with silica sand in a molding box. Each alloy was poured at 100 ± 5 °C of superheat.

Cooling curves were recorded by using a chromel alumel (type K) thermocouple located at 5 cm from the bottom of the mould in two different positions with respect to the symmetry axis. Thermocouple tips were in direct contact with the melt under study. Cooling curves were obtained by recording temperature changes as a function of time using a data acquisition system. A calibration procedure was performed with 99.99 wt.% Sn. Experimental cooling curves were numerically processed using the FTA method in order to obtain information on the solidification kinetics of the alloys under study.

Solidified rods were sectioned close to the tip of the thermocouples and their final positions were measured. Cross sections of the specimens were metallographically prepared and etched with 100 mL H_2O, 2 mL HCl, 10 g $FeCl_3$ (eutectic and hypereutectic alloys) and 10 mL acetic acid, 10 mL HNO_3, and 40 mL glycerol (hypoeutectic alloy). Microstructural observations were carried out by optical microscopy and scanning electron microscopy.

3. Results and Discussion

Figure 1 shows cooling curves associated with the three Pb-Sn alloys under study. As can be seen, cooling curves associated to hypoeutectic and hypereutectic alloys show four cooling stages. The first stage corresponds to the cooling of the superheated liquid and shows a continuous decrease in liquid temperature until the primary phase starts its solidification. After this, the cooling curve slope decreases due to the latent heat released. This trend continues until eutectic solidification starts, where cooling curves show an eutectic plateau at 183 °C. After the end of solidification, temperature of the solid alloy decreases again continuously to room temperature. The cooling curve of the eutectic alloy shows only three cooling stages including cooling of liquid, eutectic solidification, and cooling of solid.

It is well known that undercooling of each main microconstituent at the beginning of solidification is intimately related to the associated nucleation events. In the presence of nucleation barriers, the magnitude of the undercooling required to start solidification increases. Then, it is interesting to compare, using the experimental cooling curves shown in Fig. 1, the magnitude of the undercooling at the beginning of eutectic solidification. From the figures the presence of relatively high undercooling preceding the eutectic plateau for hypoeutectic and eutectic alloys can be observed. In these alloys, the eutectic melt solidifies from an undercooled state. On the other hand, for the hyper eutectic alloy (Fig. 1b), a Sn-rich primary phase in the hypereutectic alloy practically eliminates the initial eutectic undercooling observed in hypoeutectic and eutectic alloys.

This thermal behavior suggests that the Sn-rich primary phase acts as an effective substrate for nucleation of the Pb-Sn

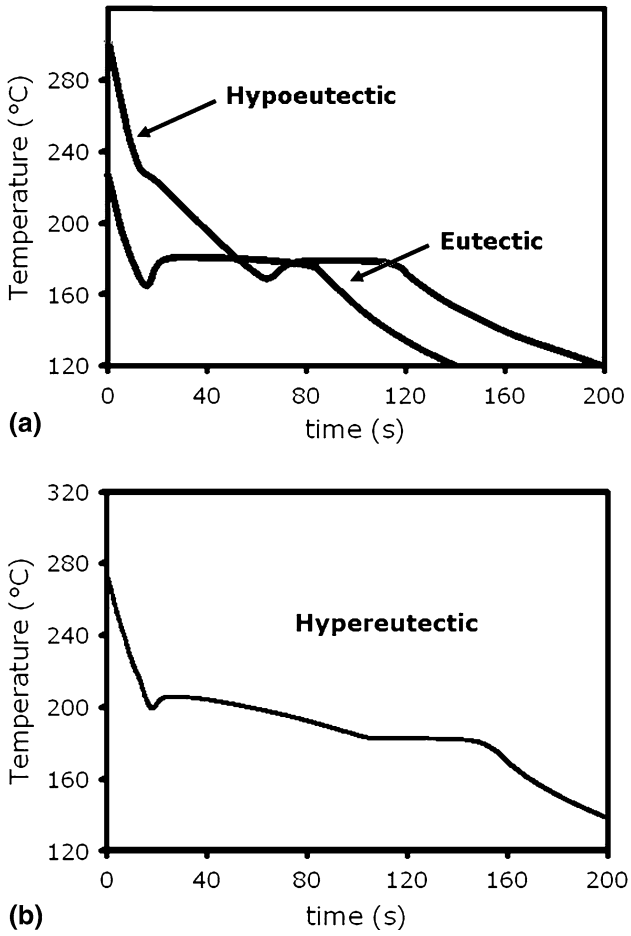

Fig. 1 Typical cooling curves of the Pb-Sn alloys: (a) hypoeutectic and eutectic alloys and (b) hypereutectic alloy

eutectic microconstituent. In the presence of the Pb-rich primary phase or for the alloy of eutectic composition, the eutectic microconstituent nucleates in the presence of important nucleation barriers, as can be inferred from the observed eutectic undercoolings.

Examination of the microstructure indicates a lamellar morphology for the eutectic microconstituent of the hypereutectic alloy (see Fig. 2a), where the pro eutectic dendrites of dark phase rich in Sn and lamellar eutectic at the interdendritic regions can be observed. On the other hand, an eutectic with the so-called anomalous morphology is observed in the hypoeutectic alloy (Fig. 2b). Here, the anomalous eutectic, which shows rounded regions of light phase rich in Pb embedded in a dark, coherent phase rich in Sn, is located at the interdendritic spaces left by primary dendrites of solid solution rich in Pb. The eutectic alloy shows the presence of both lamellar and anomalous eutectic (Fig. 2c).

FTA procedure was applied to experimental curves of these three alloys to obtain quantitative information on the operating solidification rates during eutectic solidification. Figure 3 shows evolutions of solidification rates (df_s/dt) for the cases of interest, which were obtained by numerical processing of the experimental cooling curves using the FTA method. On the same figures, the associated cooling curves are superimposed to allow an easy interpretation of FTA results.

As can be seen from Fig. 3, and focusing the attention on the FTA results during eutectic solidification (i.e., after 100 s,

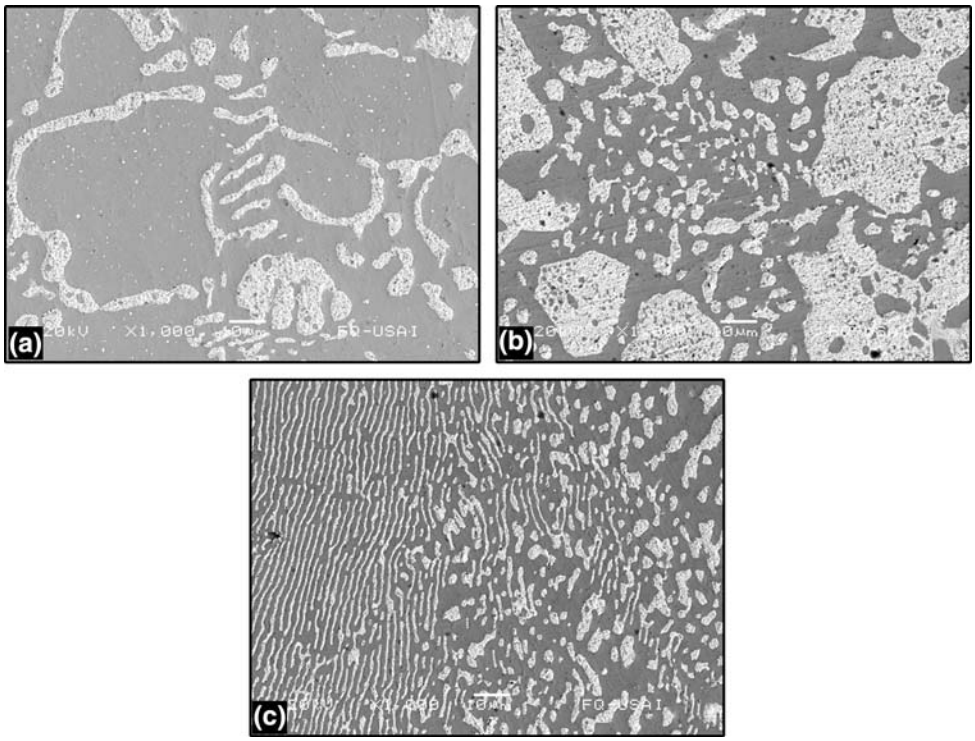

Fig. 2 SEM backscattered electron images of (a) hypereutectic, (b) hypoeutectic, and (c) eutectic solidified alloys

Fig. 3a, 50 s, Fig. 3b, and approximately 10 s, Fig. 3c), the solidification rates in hypereutectic alloy remain approximately the same during eutectic solidification. Hypoeutectic and eutectic alloys show relatively high solidification rates at earlier stages of eutectic solidification followed by rates of the same magnitude as observed in the hypereutectic alloys (i.e., around 0.01-0.02 s^{-1}). This indicates that an important part of eutectic solidification has occurred for these alloys (hypoeutectic and eutectic) under high undercooling conditions. It is interesting to note that in the case of samples that show the presence of anomalous eutectic (see Fig. 2b and c), FTA processing of the corresponding cooling curves shows relatively high solidification rates at earlier stages of eutectic solidification (see Fig. 3b and c).

Apparently, for the alloys under study, lamellar eutectic can only be formed when there is an adequate substrate, such as the primary Sn-rich primary phase present in hypereutectic alloys, avoiding the presence of high undercooling and high solidification rates during eutectic solidification and then avoiding anomalous eutectic formation.

Figure 4 shows undercooling and solidification rate evolution as a function of solid fraction for the eutectic alloy as revealed from FTA processing of the associated experimental cooling curves. Here, it can be seen (Fig. 4a) that solid formation occurs under different undercooling conditions during solidification. At the beginning and apparently due to the presence of energetic barriers to eutectic nucleation, undercooling reaches a maximum (see point a in Fig. 4a). Then, high undercooling activates nucleation and eutectic grow begins. Owing to the large driving force for crystallization accumulated as a result of the increasing undercooling at the beginning of eutectic solidification, the solidification rate is high and reaches a maximum at point d (Fig. 4b). The rapid release of latent heat causes a progressive decrease in undercooling (path b-c in Fig. 4a), which in turn reduces the solidification rate to a minimum (point e in Fig. 4b), at a solid fraction near to 0.4. The remaining of the liquid melt solidifies under relatively low undercooling and solidification rates (Fig. 4a and b).

Figure 4(b) and 2(c) suggest that during eutectic solidification of the eutectic alloy, there is a primary eutectic formed during recalescence at high undercooling and solidification rate and subsequent eutectic yielded at low undercooling and relatively low solidification rate at the eutectic plateau temperature after recalescence. This behavior is typical for eutectic solidification from undercooled melts which is commonly achieved suppressing nucleation by using experimental techniques such as containerless levitation or flux processing techniques (Ref 6). This evidence suggests that the cause behind the observed differences in the eutectic morphologies of the experimental alloys lies on the nucleating ability of the primary phase available as a potential substrate for nucleation of the eutectic microconstituent.

Using the aforementioned techniques it has been found that there are several eutectic alloys that exhibit a progressive morphology transition from the regular lamellae to a purely anomalous eutectic with an increasing undercooling acting during its solidification from undercooled melts. In the case of Pb-Sn eutectic, it was found (Ref 7), using the fluxing technique, that only when the eutectic solidifies under acting undercooling lower than 6 °C the eutectic solidifies with a near equilibrium lamellar microstructure. Otherwise, the presence of anomalous eutectic is detected in the sample. A recent work on Pb-Sn eutectic (Ref 8) has shown that by increasing undercooling three major microstructure transitions are observed. These transitions include morphological changes of the eutectic constituent from lamellar to anomalous at low undercooling levels, and morphological changes of primary α-Pb phase from

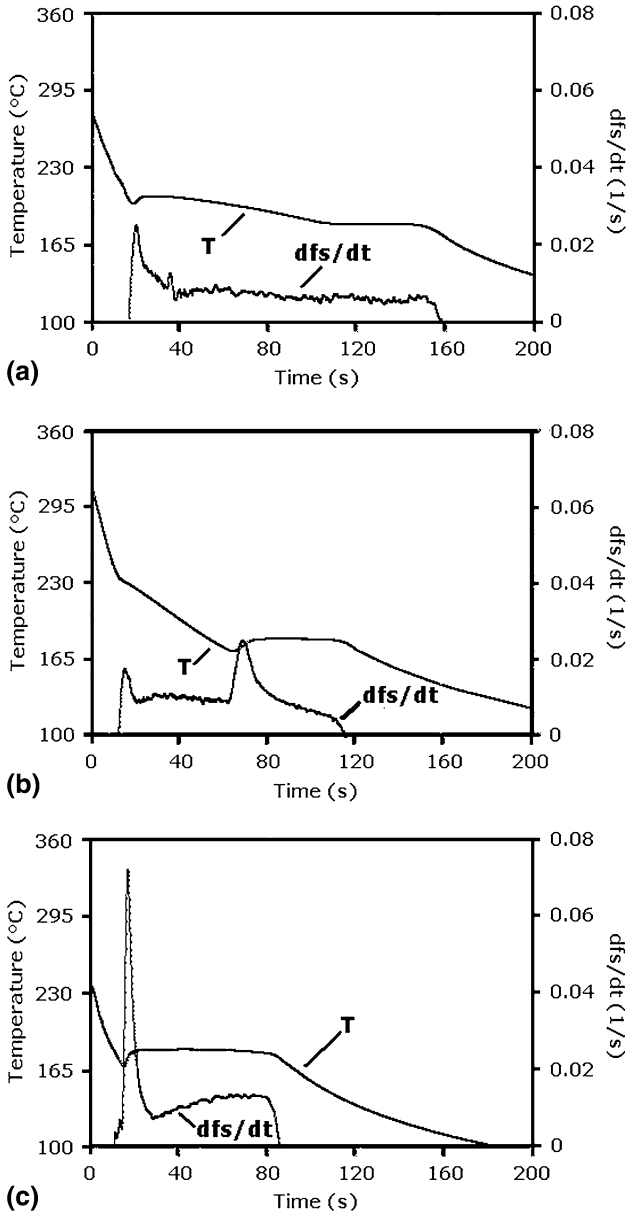

Fig. 3 Cooling curves and FTA solidification rate evolution of (a) hypereutectic, (b) hypoeutectic, and (c) eutectic alloys

dendrite to equiaxed grains at high undercooling levels are observed.

Several mechanisms have been proposed to explain the presence of anomalous eutectic during eutectic solidification in undercooled melt. One of the more accepted theories (Ref 13) claims that during formation of primary eutectic at high undercooling a fine lamellar eutectic microstructure with a high amount of interfacial energy stored forms directly from undercooled melt. Since lamellar eutectic formed during recalescence contains a high density of eutectic interfaces, they will be partially remelted and disintegrated into anomalous eutectics during solidification of the remnant liquid after recalescence.

This could explain the coexistence of lamellar and anomalous eutectic which can be observed clearly in the SEM micrograph of the eutectic probe shown in Fig. 2(c). In this figure, the lamellar regions with very fine spacings and

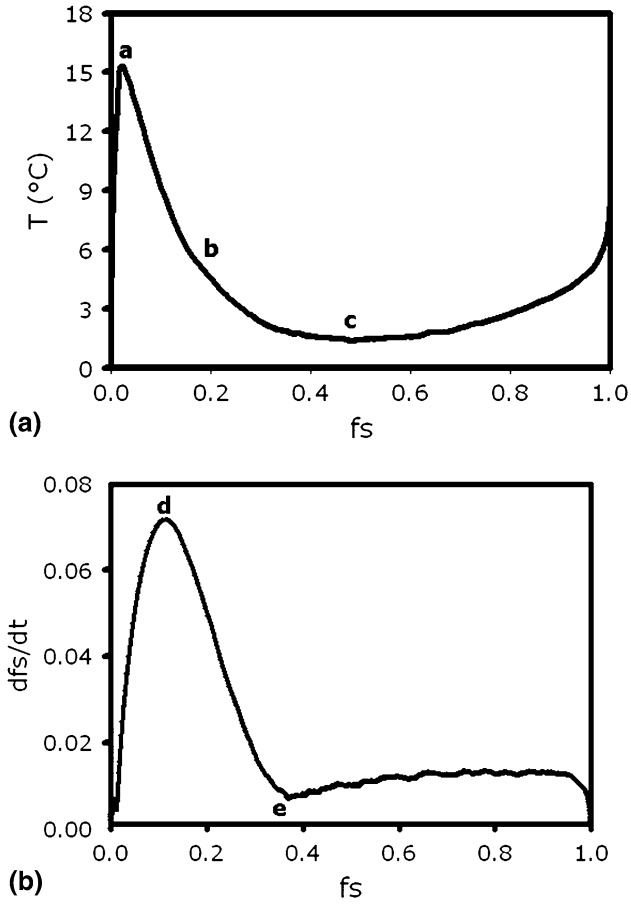

Fig. 4 Eutectic undercooling (a) and solidification rate (b) as a function of solid fraction obtained from FTA processing of the experimental cooling curves of the Pb-Sn eutectic sample

anomalous eutectics showing apparently partial remelting and disintegration of the eutectic Pb-rich phase can be seen.

However, in the case of hypoeutectic alloy, the presence of lamellar eutectic is not detected anywhere. This could mean that partial remelting and disintegration could not be the only mechanism acting during anomalous eutectic formation.

Wei et al. (Ref 14) suggest that the development of anomalous eutectic microstructures may be the result of cooperative dendritic growth of the independently nucleating eutectic phases at high undercooling, which forms, during recalescence, a two phase composite skeleton infiltrated within the remnant melt to be solidified slowly. More recently, Li and Kuribayashi (Ref 15, 16) have discussed anomalous eutectic formation in undercooled melts for eutectics formed by phases showing remarkable differences in growth kinetics. When there is a constraint on the growth of one of the eutectic phases, it is possible that the other continue its growing. This leading phase will eventually grow freely into the undercooled melt and yield decoupled growth, and under the chemical composition limitation of a eutectic alloy, it may develop into an irregular network in a three-dimensional array. When the solidified sample is sectioned, a two-dimensional microstructure is revealed where the leading phase is discontinuous and the other phase is continuous.

In the case of the hypoeutectic alloy, it is observed that the continuous phase in the anomalous eutectic is the Sn-rich solid solution. It could be that, during eutectic solidification, the

eutectic Pb-rich phase continues its growth on the preexistent Pb-rich primary phase, forming a solid skeleton or irregular network according to the abovementioned theories while the Sn-rich phase is unable to nucleate until the maximum undercooling is reached and recalescence starts. Further work is needed to explain anomalous eutectic formation in hypoeutectic Pb-Sn alloys.

4. Conclusions

Microstructural characterization of the experimental alloys shows that the primary phase formed before eutectic solidification can have an important influence defining the morphology of the eutectic microconstituent. The Pb-Sn eutectic shows lamellar morphology only in the case of hypereutectic alloy, where a Sn-rich primary phase acts as an effective substrate for nucleation of the eutectic microconstituent. For the hypoeutectic alloy, the eutectic microconstituent shows an anomalous morphology and the eutectic alloy shows both anomalous and lamellar eutectic.

FTA of the experimental cooling curves shows the presence of two solidification regimes for the eutectic formed during solidification of the hypoeutectic and eutectic alloys. The first is the solidification of primary eutectic formed at large undercooling and during recalescence while the second corresponds to a secondary eutectic formed after recalescence at low undercooling at the eutectic plateau temperature. This result shows that the observed differences in eutectic morphologies of the experimental alloys lie on the nucleating ability of the primary phase available as a potential substrate for nucleation of the eutectic microconstituent.

Experimental results suggest that partial remelting and disintegration could not be the only mechanism acting during anomalous eutectic formation.

Acknowledgments

The authors acknowledge the DGAPA (UNAM) for the financial support and A. Amaro, I. Puente, I. Beltran, and C. Atlatenco for their valuable technical assistance.

References

1. B.E. Sundquist and L.F. Mondolfo, Heterogeneous Nucleation in the Liquid to Solid Transformation in Alloys, *Trans. AIME*, 1961, **221**, p 157–164
2. S.T. Bluni, M.R. Notis, and A.R. Merder, Nucleation Characteristics and Microstructure of Eutectic Al-Zn Alloys, *Acta Metall. Mater.*, 1995, **43**(5), p 1775–1782
3. W.B. De Castro and C.S. Kiminami, Heterogeneous Nucleation Behavior in Undercooled Sn-Bi Alloys, *J. Mater. Sci. Lett.*, 1999, **18**, p 487–488
4. M.G. Chu, Y. Shiohara, and M.C. Fleming, Solidification of Highly Undercooled Pb-Sn Alloy Droplets, *Metall. Trans. A*, 1984, **15A**, p 1303–1310
5. H.C. De Groth and V. Laxmanan, Bulk Undercooling, Nucleation and Macrosegregation of Pb-Sn Alloys, *Metall. Trans. A*, 1988, **19A**, p 2651–2658
6. J.F. Li, W.Q. Jie, S Zhao, and Y.H. Zhou, Structural Evidence for the Transition from Coupled to Decoupled Growth in the Solidification of Undercooled Ni-Sn Eutectic Melt, *Metall. Mater. Trans. A*, 2007, **38A**, p 1806–1816
7. W.B. De Castro, M de Lucena, C.S. Kiminami, and C. Bolfarini, Microstructure of Undercooled Pb-Sn Alloys, *Mater. Sci. Eng. A*, 2001, **304-306**(1-2), p 255–261
8. H. Kang and W. Yoon, Microstructural Morphology Changes of the Lead-Tin Eutectic Alloy by Different Undercooling Levels, *Mater. Trans.*, 2004, **10**, p 2956–2959
9. W. Kapturkiewicz, A. Burbielko, and H.F. Lopez, A New Concept in Thermal Analysis of Castings, *AFS Trans.*, 1993, **101**, p 505–511
10. J.O. Barlow and D.M. Stefanescu, Computer Aided Cooling Curve Analysis Revisited, *AFS Trans.*, 1997, **105**, p 339–354
11. E. Fras, W. Kapturkiewicz, A. Burbielko, and H.F. Lopez, Numerical Simulation and Fourier Thermal Analysis in High Carbon Fe-C Alloys, *Metall. Mater. Trans. B*, 1997, **28B**, p 115–123
12. D. Emadi and L. Whiting, Determination of Solidification Characteristics of Al-Si Alloys by Thermal Analysis, *AFS Trans.*, 2002, **110**, p 285–296
13. R. Goetzinger, M. Barth, and D.M. Herlach, Mechanism of Formation of the Anomalous Eutectic Structures in Rapidly Solidified Ni-Si, Co-Sb and Ni-Al-Ti Alloys, *Acta Mater.*, 1998, **46**(5), p 1647–1655
14. B. Wei, D.M. Herlach, B. Feuerbacher, and F. Sommer, Dendritic and Eutectic Solidification of Undercooled Co-Sb Alloys, *Acta Metall. Mater.*, 1993, **41**(6), p 1801–1809
15. M. Li and K. Kuribayashi, Nucleation-Controlled Microstructures and Anomalous Eutectic Formation in Undercooled Co-Sn and Ni-Si Eutectic Melts, *Metall. Mater. Trans. A*, 2003, **34A**(12), p 2999–3008
16. M. Li and K. Kuribayashi, Further Discussion on the Free Growth Behavior in the Solidification of Undercooled Eutectic Melts, *Metall. Mater. Trans. A*, 2003, **34A**(6), p 1393–1396